On the mechanism of the hydrogen-induced exfoliation of silicon

M. K. Weldon, V. E. Marsico, Y. J. Chabal, A. Agarwal,[a] D. J. Eaglesham, J. Sapjeta,
W. L. Brown, D. C. Jacobson, Y. Caudano, S. B. Christman, and E. E. Chaban
Bell Laboratories, Lucent Technologies, 600 Mountain Avenue, Murray Hill, New Jersey 07974

We have investigated the fundamental mechanism underlying the hydrogen-induced exfoliation of silicon, using a combination of spectroscopic and microscopic techniques. We have studied the evolution of the internal defect structure as a function of implanted hydrogen concentration and annealing temperature and found that the mechanism consists of a number of essential components in which hydrogen plays a key role. Specifically, we show that the chemical action of hydrogen leads to the formation of (100) and (111) internal surfaces above 400 °C via agglomeration of the initial defect structure. In addition, molecular hydrogen is evolved between 200 and 400 °C and subsequently traps in the microvoids bounded by the internal surfaces, resulting in the build-up of internal pressure. This, in turn, leads to the observed "blistering" of unconstrained silicon samples, or complete layer transfer for silicon wafers joined to a supporting (handle) wafer which acts as a mechanical "stiffener." © *1997 American Vacuum Society.* [S0734-211X(97)08904-X]

I. INTRODUCTION

The physics and chemistry of hydrogen in silicon has been the subject of considerable scientific and technological interest for over three decades. This interest has been driven, in part, by the ubiquitous occurrence of hydrogen in semiconductor processing which invariably leads to incorporation into the substrate either intentionally or unintentionally. Importantly, this hydrogen may profoundly alter the electrical characteristics of the resultant device by diffusion into the active region and passivation of the dopant. The myriad studies of hydrogen that have resulted are summarized in a number of review texts, to which the reader is referred for a comprehensive treatise.[1–3]

Recently, there has been renewed focus on the internal transformations that occur upon implantation of hydrogen into semiconductors due to the demonstration of the hydrogen-induced shearing of macroscopic layers of silicon, with complete transfer to a supporting wafer to which the implanted material had previously been joined.[4] In this way, it was found that thin (1000 Å − 2 μm), crystalline films of Si could be formed on top of an SiO_2 layer which was itself bonded to another Si wafer (the support or "handle"). That is to say that extremely high-quality silicon-on-insulator (SOI) structures could be formed directly during annealing (as schematically illustrated in Fig. 1), with vastly improved thickness uniformity [total thickness variation (TTV) = ±50 Å over a 100 mm wafer] relative to that obtained using conventional wafer bonding technology, for which extensive grinding and etching is required to form the final, thin silicon layer.[5] This remarkable process has also subsequently been applied to the transfer of thin layers of exotic materials (e.g., SiC, InP) onto supporting wafers and therefore shows real promise as a generally applicable material synthesis protocol.

Despite the potential importance of this process, the fundamental phenomena that drive the layer shearing and dictate the quality of the transferred layer, remain poorly under- stood. For example, it is not known whether the principal role of hydrogen is "chemical," i.e., it passivates the internal Si dangling bonds preventing reformation of Si–Si linkages or facilitates bond scission by concomitant insertion into the Si–Si bonds. In this case, the relative kinetics/ thermodynamics of the Si–H species formed will strongly influence the internal structure that develops upon annealing. Alternatively, the dominant process may be "physical/ mechanical" in nature, in that the creation of internal pressure by H_2 formation, combined with the damage caused by the implanted hydrogen may effectively cause fracture of the Si substrate. If so, the recombination kinetics of dihydrogen formation (which may, in turn, depend on the transport or diffusion of H from point defects), or the development of appropriate regions of free space (i.e., voids) in which to evolve the H_2 gas, may dictate the rate of exfoliation. Clearly, much remains to be resolved at the microscopic and macroscopic level.

Therefore, we have undertaken a wide-ranging series of studies of the thermal evolution of hydrogen implanted into silicon, as a function of implantation dose, depth, and annealing temperature, the results of which are summarized in this article. Using a combination of infrared (IR) spectroscopy, forward recoil scattering (FRS), transmission electron microscopy (TEM), and atomic force microscopy (AFM), we have been able to elucidate the key transformations that occur in both nonbonded and bonded silicon substrates. Specifically, we find that the mechanism consists of the following essential components (i) Initial formation of hydrogenated point defects complexes in the regions of lower hydrogen concentration (i.e., at the periphery of the implanted region), as well as extensive disruption of the silicon lattice (due to multivacancy formation) and 50–100 Å platelet formation near the peak of the implantation profile;

1) Ion implantation
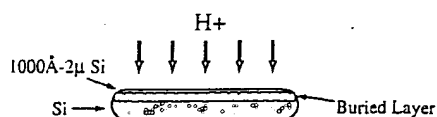
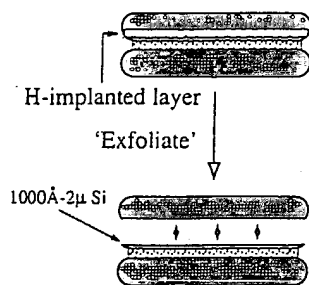

2) Invert, Bond and Anneal

FIG. 1. Schematic illustration of the commercial SmartCut™ process, in which an oxidized Si wafer is preimplanted with H$^+$, then subsequently joined to a second (handle) wafer and annealed, resulting in the direct formation of a high quality SOI substrate.

(ii) Collapse of this defective, multivacancy structure resulting in formation of H_2 and agglomeration of the remaining bound hydrogen into vacancy defect complexes such as $VH_{3,4}$ upon annealing to 400 °C; (iii) Rearrangement of the defect structure above 400 °C into extended internal hydrogen-terminated (100) and (111) surfaces; (iv) Trapping of H_2 in the microvoids bounded by the internal surfaces, resulting in the build-up of internal pressure; (v) Development of these microvoids into macroscopic (pressurized) cracks that either lead to blistering of unconstrained silicon samples, or complete layer transfer for silicon wafers joined to a supporting (handle) wafer. We show that the role of the handle wafer is to provide the necessary restoring force to drive crack propagation parallel to the surface, effectively suppressing the vertical lift off that leads to blistering.

II. EXPERIMENT

All studies were performed on Si(100) wafers [100 mm FZ, boron doped (p type), resistivity 5–10 Ω cm] implanted with H$^+$ (through a 3000 Å layer of thermally grown oxide) at doses ranging from 2×10^{16} to 1.8×10^{17} H/cm^2 and energies ranging from 75 keV to 1 MeV, resulting in implantation depths of 3300 Å to 16 μm. The substrate was maintained at close to ambient temperature throughout the implantation. The samples were given a modified RCA clean prior to analysis to remove surface contaminants introduced by the implantation process. Finally, some of the implanted samples were joined to an unimplanted handle wafer that was terminated by the thin chemical oxide layer formed by the RCA clean.[6,7] All wafers were cut into smaller samples for analysis. Annealing was performed sequentially for 30 min at each temperature in a tube furnace either under vacuum ($P \sim 2 \times 10^{-8}$ Torr) or a positive pressure of N_2. No

dependence on the anneal ambient (vacuum or N_2) was found, but the shearing/layer transfer process was found to be a sensitive function of the annealing protocol and thermal history of the sample.

The infrared data were obtained using a Nicolet 60 SX FTIR spectrometer equipped with a broadband MCT detector and operating at 2 cm^{-1} resolution in a multiple internal reflection (MIR) geometry. All spectra were collected under ambient conditions and referenced either to an identical unimplanted sample or an implanted sample that had previously been annealed to 1100 °C, at which temperature no hydrogen remains. Additional baseline subtraction was usually required to remove oscillations that result from interference between beams reflected from the implanted region (after partial separation/crack development) and the sample surface. In each case, this subtraction was performed using the same high order polynomial function that was fit to the entire broadband spectrum (1500–8000 cm^{-1}) to minimize the preferential selection of spectral features.

Samples for cross-sectional imaging by transmission electron microscopy (TEM) were prepared in the conventional way by mechanical thinning and Ar$^+$ ion beam milling. The H implantation-induced damage and defects were imaged in bright field and dark field conditions using the weakly excited 400 reflection, and in axial [110] high resolution.

Forward recoil scattering studies were performed using 2.6 MeV He$^+$ ions incident at 15° to the surface plane and recoiled H was detected at 30° to the incident beam direction. Concentration calibration was performed by comparison to a standard sample implanted with a known hydrogen concentration.

Atomic force microscopy (AFM) was performed using a Nanoscope III (Digital Instruments, Santa Barbara, CA) in either contact or tapping mode. Large-scale images (≥ 25 μm$\times 25$ μm) were obtained in contact mode with silicon nitride tips. Roughness values of the exfoliated and substrate surfaces were determined using a tapping mode with etched silicon tips. The reported roughness value is the average of six measurements made at different scan sizes ranging from 0.1 to 5 μm.

III. RESULTS AND INTERPRETATION

A. Infrared spectroscopy

Representative spectra for both a low dose (2×10^{16} H/cm^2) and an intermediate dose (6×10^{16} H/cm^2) of hydrogen implanted into Si(100) are shown in Fig. 2, as a function of annealing temperature. For the as-implanted low dose sample, the 1800–2300 cm^{-1} region consists of at least 11 discrete Si–H stretching modes, superimposed on a broadband centered at ~ 2000 cm^{-1}. Similar features are observed for the intermediate dose; however, the intensity of broadband absorption is increased markedly, so that it dominates the discrete mode structure. The origin of these two types of spectral features (that are common to all H$^+$ doses that we have studied) can be assigned in a qualitative sense by reference to the extensive literature. Although the precise
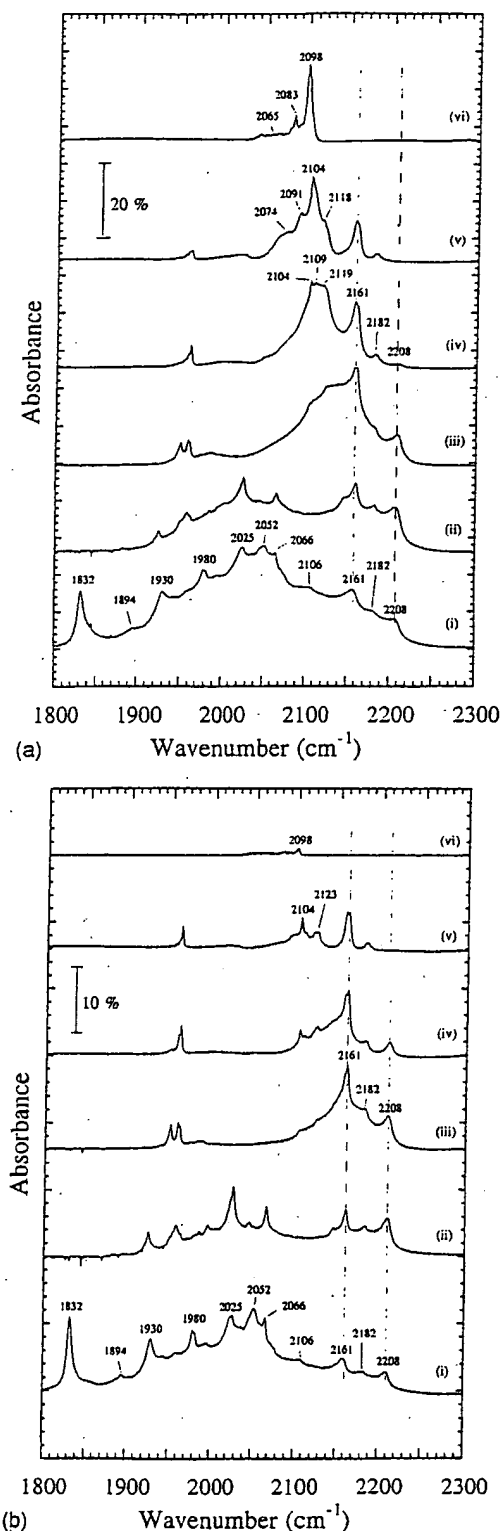
(a)   Wavenumber (cm^{-1})

(b)   Wavenumber (cm^{-1})

FIG. 2. Infrared spectra of the Si–H stretching modes of hydrogen implanted 3300 Å into Si(100) at doses of (a) 6×10^{16} H/cm^2 (intermediate dose) and (b) 2×10^{16} H/cm^2 (low dose) at (i) room temperature and after annealing to: (ii) 300 °C; (iii) 425 °C; (iv) 500 °C; (v) 550 °C; and (vi) 650 °C.
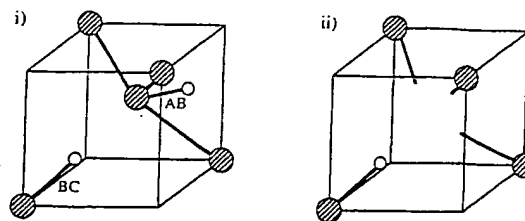

FIG. 3. Illustration of (local) Si–H defects observed in this work; (i) H$_2^*$ defect and; (ii) Monovacancy monohydride VH (VH$_{3,4}$ have 3 and 4 of the dangling bonds of the monovacancy terminated with H, respectively). Larger shaded circles=Si; smaller open circles=H.

denote a Si vacancy, "I" denotes a Si interstitial, and the subscripts may have the values $x=1$ and 2 and $y=1-4$), imbedded in crystalline silicon, whereas the broad absorption is due to H trapped in a highly defective Si region. In fact, this broadband absorption is strongly reminiscent of that observed for hydrogenated amorphous silicon, a:Si–H, which has been attributed to a inhomogeneous distribution of monohydride-terminated, multivacancy defects also of the form V$_x$H$_y$, but with $x=3$ or 4 and $y=1$.[1] In accordance with this assignment, we ascribe the band centered at 2000 cm^{-1} to such a "multivacancy" defect region.

From our studies of a wide variety of different H$^+$ doses and depth distributions, we find that the point defect mode intensity is largely invariant with dose, whereas the multivacancy signature scales with the hydrogen concentration, so that it is probable that the point defects occur at the periphery of the multivacancy region which, in turn, occurs around the peak of the hydrogen concentration profile. The specific assignments of some of these point defect modes are still somewhat controversial; however, it is instructive to consider the nature of the modes for which more definitive assignments can be made, before continuing to discuss the annealing data.

The pair of modes observed at 1832 and 2052 cm^{-1} in the as-implanted samples are assigned to the H$_2^*$ defect [Fig. 3(a)], by reference to the detailed studies of this species by Bech Nielsen *et al.*[3] Specifically, the two Si–H modes are due the (weakly) coupled motions of a hydrogen atom bound close to the bond center (BC) site in the Si lattice (2052 cm^{-1}) and the other at the antibonding (AB) site (1832 cm^{-1}). Importantly, the close agreement between the frequencies and annealing behavior ($T<250$ °C) observed in this work, with those previously reported in the literature (1838/2062 cm^{-1} and $T<250$ °C), strongly support this assignment.

In addition, the modes observed above 2050 cm^{-1} are primarily assigned to hydrogen bound at monovacancy defects of the form VH$_y$ where $y=1-4$ [Fig. 3(b)], by reference to the literature. Recent isotopic labeling studies, in combination with uniaxial stress measurements of proton-implanted Si have afforded the following assignments:[6] The feature at 2066 cm^{-1} is assigned to a single hydrogen bound to the monovacancy defect (VH); the features at 2161 and

assignment of each specific feature is still the subject of considerable controversy,[1] there is general consensus that the discrete modes are associated with isolated point defect type complexes of the form V$_x$H$_y$ or Si$_I$H$_y$ (where "V" is used to

$2182 \, cm^{-1}$ are due to three hydrogen atoms bound to the monovacancy (VH_3), whereas the $2208 \, cm^{-1}$ band is due to VH_4.[7] The feature at $2106 \, cm^{-1}$ is intriguing as it occurs in the frequency range usually ascribed to hydrogen bound to extended Si surfaces (see the following). Therefore, given that TEM images of the as-implanted sample show (111) and (100) "seed" platelets (Sec. II), we tentatively assign this feature to hydrogen terminating these 50–100 Å platelets. Finally, the bands at 1930 and $2025 \, cm^{-1}$ are assigned to small divacancy clusters terminated by either one or two hydrogens, i.e., V_2H or V_2H_2.[1] Now, considerable progress can be made in understanding the broad transformations that occur upon annealing, based on these assignments and our recent definitive proof of the origin of modes that appear at ~$2100 \, cm^{-1}$ at higher temperatures,[8] as summarized below.

There is a general attenuation of the broadband, multivacancy structure after annealing to 300 °C, as well as the complete loss of the H_2^* modes at 1832 and $2052 \, cm^{-1}$. In contrast, the VH_3 and VH_4 multiply-hydrogenated monovacancy modes at 2161/2182 and $2208 \, cm^{-1}$, respectively, are all enhanced relative to the as-implanted spectrum. Based on these observations, we can immediately conclude that there is both a net loss of *bound* hydrogen and agglomeration of the remaining trapped hydrogen at existing vacancies. These initial trends are exacerbated after annealing to 425 °C for both samples [Figs. 2(a)(iii) and 2(b)(iii)]. Essentially complete attenuation of the multivacancy signature occurs, together with a pronounced growth of the agglomerated hydrogen monovacancy modes discussed above, so that the latter modes dominate the observed spectrum. After annealing to higher temperatures, the similarity in the evolution of the features for the low and intermediate H^+ doses disappears. Most notably, for the $6 \times 10^{16} \, H/cm^2$ dose the monotonic loss of the VH_3 and VH_4 modes is accompanied by the growth of discrete spectral features at $2100–2120 \, cm^{-1}$, which we will show have profound mechanistic implications. In contrast, the spectra of the $2 \times 10^{16} \, H/cm^2$ dose simply show attenuation of the agglomerated monovacancy modes, with almost no attendant growth of new spectral features.

Specifically, new modes appear at 2104, 2109, and $2119 \, cm^{-1}$ in the spectrum of an intermediate hydrogen dose annealed to 500 °C [Fig. 2(a)(iv)]. Upon further annealing to 550 °C, the two higher frequency peaks collapse, leaving only the sharp $2104 \, cm^{-1}$ feature [Fig. 2(a)(v)] with a distinct shoulder at $2091 \, cm^{-1}$ and a broader band centered at $2074 \, cm^{-1}$. Finally, at 650 °C, the $2104 \, cm^{-1}$ mode is replaced by an even sharper peak at $2098 \, cm^{-1}$ and a new discrete feature is apparent at $2083 \, cm^{-1}$ [Fig. 2(a)(vi)]. The assignment of these features is central to the understanding of the exfoliation process, since they develop coincident with the appearance of surface blistering in these (nonbonded) samples. More importantly, this blistering is not observed for the low dose, $2 \times 10^{16} \, H/cm^2$ sample for which these vibrational modes are demonstrably absent. Conversely, the appearance of modes at ~$2100 \, cm^{-1}$ occurs at lower temperatures for doses of 1.0×10^{17} and 1.8×10^{17}, for which the

onset of blistering occurs at 450 and 400 °C, respectively (data not shown).

We propose that the modes at $2060–2120 \, cm^{-1}$ are due to hydrogen trapped at extended internal surfaces, based on the remarkable agreement with the known surface literature and extensive additional studies of internal hydrogen-terminated surfaces formed by wafer bonding.[9,10] A rigorous discussion of the assignment of these modes is given elsewhere,[8] the essence of which is summarized as follows: The bands at 2109 and $2119 \, cm^{-1}$ are due to the symmetric and asymmetric $Si-H_2$ stretching motions of atomically rough (100) surfaces, based on the excellent agreement with the frequencies reported for dilute HF etched Si(100), for which $\nu_{ss}(SiH_2)$ and $\nu_{as}(SiH_2)$ are observed at 2109 and $2120 \, cm^{-1}$, respectively.[11,12] The mode at $2104 \, cm^{-1}$ present at 500–550 °C is paired with the mode at $2091 \, cm^{-1}$ that is clearly resolved in the 550 °C spectrum and attributed to $\nu_{as}(SiH_2)$ and $\nu_{ss}(SiH_2)$ of atomically smoother dihydride terminated Si(100) surfaces.[13] Once again, there is precise agreement with the literature values of 2103 and $2091 \, cm^{-1}$ for dihydride prepared by UHV exposure of Si(100) to atomic hydrogen. These assignments essentially dictate that, upon further annealing, these internal surfaces should undergo the (2×1) reconstruction to produce the coupled monohydride species, $H-Si-Si-H$, just as is observed for hydrogen-terminated Si(100) surfaces in UHV. Indeed, this is precisely what is observed; the modes at 2098 and $2074 \, cm^{-1}$, observed above 550 °C, are characteristic[14] of coupled monohydride species on the atomically smooth terraces and along the steps of a Si(100) surface, respectively!

Finally, the sharp mode at $2083 \, cm^{-1}$ in the spectrum of $6 \times 10^{16} \, H/cm^2$ annealed to 650 °C, can be definitively assigned to an atomically flat Si(111) surface.[15] In fact, the weak broadband structure observed at lower frequency (~$2065 \, cm^{-1}$) has recently been assigned to the coupled mode formed by two opposing, *closely interacting* $H-(1 \times 1)Si(111)$ surfaces.[10] Both theoretical and experimental studies of the bonding of two such surfaces clearly demonstrate that when the intersurface separation approaches ~1–2 Å, the van der Waals interaction gives rise to a perturbed mode at $2065 \, cm^{-1}$, in addition to the unperturbed mode at $2083 \, cm^{-1}$. Finally, we have recently obtained further confirmation of the internal surface character of these modes by studying the low frequency, bending modes (~615–650 cm^{-1}) associated with these $Si-H$ stretching frequencies[8] and we find that, once again, there is excellent agreement with the data obtained for hydrogen-terminated Si(111) and (100) surfaces.

B. Transmission electron microscopy

We have also studied the thermal evolution of the implanted region using cross-sectional TEM, in order to establish the existence of internal (100) and (111) extended defects. In Fig. 4, a typical electron micrograph of the as-implanted region is shown, together with an image obtained after annealing a sample implanted with $1 \times 10^{17} \, H/cm^2$ to

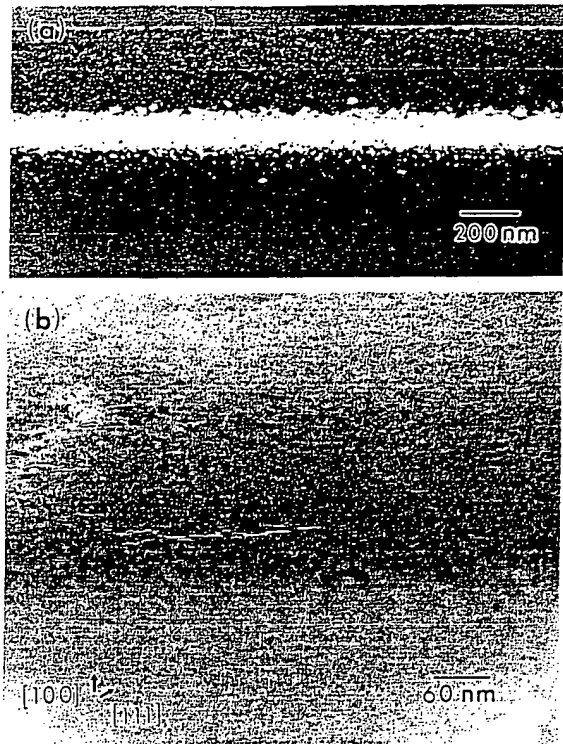FIG. 4. Cross-sectional TEM images of Si(100) implanted with 1 × 10^{17} H/cm^2 after; (a) room temperature implantation and; (b) annealing to 475 °C [image obtained with higher magnification than (a)].

FIG. 5. (a) Optical micrograph of 1 × 10^{17} H/cm^2 after annealing to 475 °C (Mag. × 90). (b) AFM image of a 15 μm × 15 μm region of the same sample as in (a).

475 °C. The as-implanted image shows a highly defective (but not truly "amorphous") layer, located approximately 2800–4300 Å below the surface. Both bright field and high resolution microscopy of a thinner section of the TEM foil (image not shown) reveal that the defective layer contains some plateletlike defects (50–100 Å) oriented along the (100) and (111) planes, as has been previously observed for silicon exposed to hydrogen-containing plasmas.[16] Interestingly, after annealing to 475 °C, a connected network of microcracks appears [Fig. 4(b)] forming a corrugated "macro" crack (2–3 μm in length) parallel to the (100) surface. These cracks are seen to consist predominantly of (100) planes that are connected by a minority of (111) planes, in excellent agreement with our conclusions based on infrared data.

C. Optical and atomic force microscopy

The effect of the internal crack formation on the overlying silicon has been investigated using both optical microscopy and AFM (Fig. 5). The initially pristine surface is visibly disrupted on annealing a sample implanted with 1 × 10^{17} H/cm^2 to 475 °C. The optical micrograph clearly shows the surface consists of both "popped" blisters with sizes ranging from 10 to 250 μm, and "capped" bubbles of dimension 10–70 μm. Additional information is available in the atomic force microscope image of the same sample [Fig. 5(b)]. The depth of the crater formed by this blistering can be measured and is found to be equal to the implantation depth, i.e., the peak of the implanted H concentration profile, where the crack formation is most pronounced. This observation
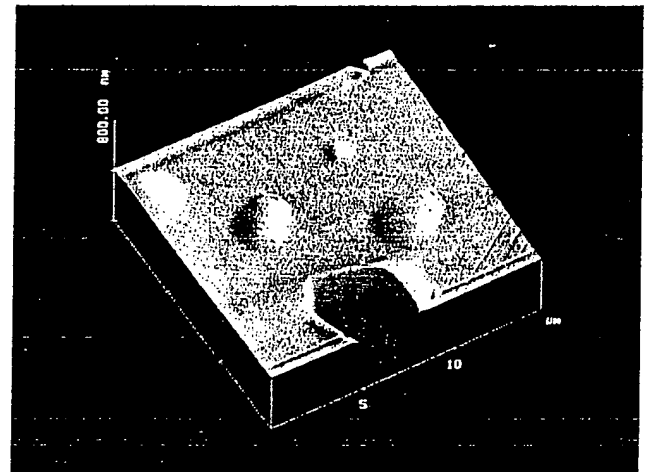
confirms the intuitive notion that the underlying cracks lead to the lift off of the overlying Si. More importantly, the presence of the capped bubbles on the Si surface strongly suggests that there is an internal pressure that causes elastic deformation of the overlying Si. In fact, using the elastic modulus of Si and assuming a bubble of dimensions 100 Å (height) × 2 μm (diameter) as observed by AFM, we estimate that the internal pressure must approach ~10 kbar, *even for capped bubbles* which, presumably, are not sufficiently pressurized to give rise to blistering. Finally, the rms roughness measured at the bottom of the crater is found to be only 80 Å, which underlines the power of this approach for high quality layer transfer.

D. Forward recoil scattering

We have employed FRS to complete the arsenal of probes used to study these samples. Importantly, it is a probe of the total hydrogen content, in contrast to IR spectroscopy which is not sensitive to the presence of molecular H$_2$ under normal
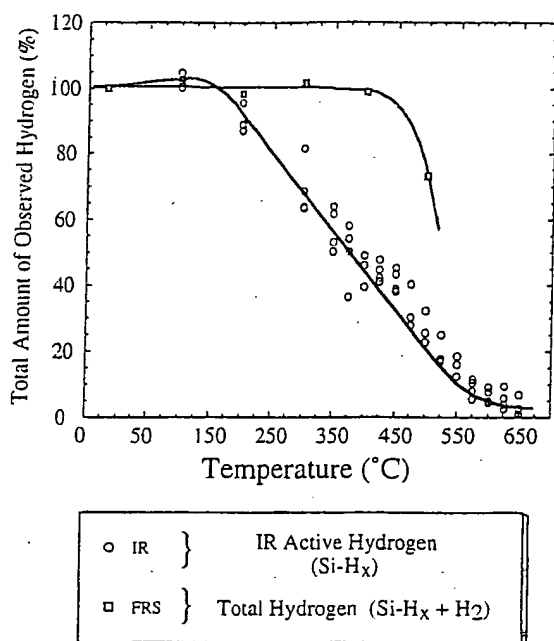
FIG. 6. Plot of the integrated hydrogen signal obtained using forward recoil scattering and IR spectroscopy.

conditions. The total amount of hydrogen, determined by FRS, is plotted as a function of annealing temperature in Fig. 6. In addition, the normalized integrated IR absorbance for each hydrogen dose is also plotted on the same axes. The disparity in the temperature dependence is immediately apparent on comparison of the data obtained using the two techniques; the amount of bound hydrogen monotonically decreases above 200 °C, while the total hydrogen content remains constant up to 400 °C. Clearly, there has been a conversion of trapped hydrogen to an unbound form, i.e., either atomic or molecular hydrogen. The existence of isolated H atoms can be effectively eliminated since it is highly improbable that such a state would be stable with respect to trapping at a vacancy or interstitial defect upon cooling to room temperature (where the data were acquired). Therefore, the only reasonable interpretation is that there is net conversion of Si–H into H_2 at temperatures between 200 and 500 °C, and that the molecular hydrogen remains trapped in the Si crystal. Interestingly, previous theoretical investigations of hydrogen in intrinsic Si found that H_2 is indeed stable at the tetrahedral interstitial sites.[17] However, the solubility of H_2 in room temperature silicon is vanishingly small.[3] In addition, the diffusion length of hydrogen in Si is greater than the implantation depth (3300 Å) over this temperature range,[1] so that the molecular hydrogen cannot be trapped in the Si lattice per se. We propose that the H_2 must be bound at internal voids or cavities, as has been observed for hydrogenated amorphous silicon (a-Si:H). Notably, molecular hydrogen was found to accumulate in the 10–20 Å pores in a-Si:H, for temperatures up to 400 °C, resulting in internal pressures as high as 100 kBar.[18] These voids are distinct from the hydrogenated $VH_{3,4}$ defects discussed above, since these monovacancy defects cannot accommo-

date a H_2 molecule. Therefore, it is probable that hydrogen traps voids of the type V_x (where $x>1$) that are produced from the initial multivacancy structure. Indeed, since these voids are not hydrogen terminated (based on the absence of any related Si–H modes observed between 200 and 350 °C), it is plausible that the H_2 is produced by recombination of the Si–H monohydride species that initially decorate the multivacancy structures, and traps locally in the hydrogen-free multivacancies so formed. In this picture, the coalescence of the initial multivacancy structure to form the agglomerated monovacancy $VH_{3,4}$ defects is a competing reaction pathway.

The last point of note is that the rate of conversion of Si–H to H_2 is equivalent for both low (2×10^{16} H/cm^2) and high hydrogen doses (1.0×10^{17} H/cm^2), i.e., the FRS and IR data show identical functional dependencies independent of dose. Yet, the samples implanted with 2×10^{16} H/cm^2 outwardly show a clear difference in their annealing behavior in that they do not give rise to exfoliation. This observation has important mechanistic implications that are discussed below.

IV. DISCUSSION

In the preceding section, the essential elements of the exfoliation process were highlighted and discussed separately. In the remainder of this article, we will combine these elements to propose a coherent mechanism that has phenomological utility.

The first important observation is that it is the "multivacancy" defect structure that produces molecular hydrogen on annealing up to 350 °C, by comparison of the integrated FRS and IR data. Specifically, the total (crystalline) point defect absorption is constant up to 350 °C, in contrast to the ~40% attenuation of the broadband component of the IR absorption over this temperature range. Subsequently, on annealing to ~400 °C, attenuation of all the vibrational features below 2100 cm^{-1} occurs, with the continued production of H_2 as well as the formation of the agglomerated $VH_{3,4}$ type defects. Both the H_2 production and $VH_{3,4}$ defect formation scale with the hydrogen dose, which necessitates that they are predominantly derived from the multivacancy region (see earlier). Furthermore, previous studies of lower hydrogen doses (1×10^{16} H/cm^2), which do not exhibit any appreciable broadband absorption at 2000 cm^{-1}, found that no IR inactive species were formed at any temperature, but reported pronounced $VH_{3,4}$ features at 2160 and 2210 cm^{-1}.[19] Therefore we conclude that only the multivacancy region yields H_2 in our studies, but that both defect regions support the growth of the agglomerated defects.

Secondly, we propose that the agglomerated $VH_{3,4}$ defects are precursors to the formation of extended internal surfaces, based on the attenuation of the former concomitant with the appearance of the latter. Moreover, it is reasonable to postulate that the initial 50–100 Å (100) and (111) platelets observed following implantation may serve to seed or nucleate the formation of the extended surfaces, by attachment of these agglomerated defect structures. In either case, the proposed role of $VH_{3,4}$ defects implies that the kinetics of inter-

nal surface formation should be a function of the density of such defects. Indeed, this is exactly what is observed experimentally; the rate of crack propagation increases with the integrated absorbance of the 2161, 2182, and 2208 cm^{-1} bands. Furthermore, there is a minimum density of VH$_{3,4}$ defects, below which efficient extended surface formation does not occur, as is manifestly the case for the low (2 $\times 10^{16}$ H$^+$/cm^2) dose.

Now, the question arises as to the exact role that the H$_2$ formation plays in the exfoliation process. We have already intimated that an internal pressure must develop in the implanted region, by observation of pressurized capped bubbles for intermediate to high hydrogen doses (Fig. 5), and that internal cracks are somehow involved, but now we will further substantiate the causal link between these observations.

The IR and TEM data clearly demonstrate the presence of the internal (100) and (111) surfaces after annealing samples implanted with 6×10^{16}–1.8×10^{17} H/cm^2 to between 350 and 450 °C. Furthermore, we find that exfoliation only occurs after the appearance of these internal surfaces/cracks and *does not occur* when the crack density is too low, i.e., for H doses of 2×10^{16} H/cm^2. In addition, the blistering is found to originate in the regions of the highest crack density, which strongly suggests that the pressure is developing in the cracks. All that remains is to prove that H$_2$ is indeed present and is the source of the internal pressure. This we have verified using *in situ* mass spectrometry during the annealing process. Specifically, we observed a massive burst of molecular hydrogen coincident with the occurrence of exfoliation, with no other gaseous products detected at any temperature. Interestingly, by careful calibration of the mass spectrometer, we were also able to quantify the total amount of H$_2$ evolved and found that only 30% of the initial H implant is liberated in this step; IR spectra of the two sheared pieces clearly demonstrate that a substantial amount of hydrogen remains trapped at internal cracks that persist beneath the newly formed surfaces (data not shown).

So, a coherent mechanism is beginning to emerge: At sufficiently high doses, implantation of hydrogen into silicon predominantly causes the formation of multivacancy structure. Upon annealing to temperatures between 200 and 350 °C, this multivacancy defect region simultaneously liberates H$_2$ and partially evolves into a small-cavity structure, which traps the H$_2$ so formed. In addition, agglomerated monovacancy defects are also produced from the initial multivacancy structure which, in turn, coalesce (or nucleate at the 50–100 Å platelets) to form internal (100) and (111) surfaces. The molecular hydrogen subsequently accumulates in the microscopic cracks that are defined by these extended surfaces, resulting in the development of sufficiently high internal pressures to cause the exfoliation of the overlying silicon. So, the role of the implanted H is twofold: (i) It acts "chemically" in that it drives the formation of microscopically flat internal surfaces and acts as a source of gaseous H$_2$ which traps in the internal cavities where; (ii) it acts "physically" as an internal pressure source.

The preceding mechanism suggests that a critical kinetic

regime exists, wherein the molecular H$_2$ is liberated from the (angstrom scale) voids and must retrap in the incipient microcracks, in order to prevent diffusion away from the implanted region and allow the creation of the requisite internal pressure. Clear evidence for this is provided by reference by the data obtained for low H doses (2×10^{16} H$^+$/cm^2), for which the crack density is found to be very low, so that the molecular hydrogen can, by the preceding analysis, escape from the implanted region and diffuse into the bulk crystalline silicon. This is indeed what is observed for such a low H dose sample when it is prejoined to a handle wafer. Specifically, the out-diffusing H$_2$ is found to accumulate in the microvoids present at the *joined* interface, upon annealing to 550 °C, resulting in the build-up of pressure and eventual separation at this interface.

These mechanistic deductions also naturally explain the slightly surprising observation that the thermal evolution of the integrated FRS/IR data are similar for both low and high H$^+$ doses, despite the vastly different crack densities observed in the two cases. This *apparent* similarity in the evolution of the implanted hydrogen, results from the similar kinetics for hydrogen out diffusion (which occurs for the 2×10^{16} H$^+$/cm^2 dose) and internal surface formation/blistering (that is dominant for the 1×10^{17} H$^+$/cm^2 dose); both of which directly result in a net loss of hydrogen on annealing to 450 °C.

Clearly, a number of key processes, i.e., crack formation, hydrogen diffusion, and H$_2$ trapping in voids, are all operative in the same temperature regime, but the question remains as to which is the *rate-limiting* step. In order to address this, we have performed a series of annealing experiments in which the time to induce exfoliation was measured as a function of different annealing temperatures for a dose of 6×10^{16} H/cm^2. Then a simple Arrhenius analysis was performed to yield an "effective" activation energy of 1.8 eV. Interestingly, it has recently been shown that the values obtained by such an analysis are in reasonably good agreement with the bond energy of the implanted material for a variety of different substrates such as Si, SiC, and diamond,[20] suggesting that the *rate-limiting step is the rupture of the remaining Si–Si bonds* in the implanted region. Indeed, the value that we obtain is close to the value of 2.3 eV for the bulk Si–Si bond energy. The fact that the value is actually ~20% lower than the nominal Si–Si bond energy is not surprising since the thermal heating serves not only to activate Si–Si bonds (as assumed in the Arrhenius analysis) but also to increase the pressure of the gas in the cracks which is not explicitly accounted for. Therefore, the value so derived should be lower than the material bond energy because the additional pressure-induced activation will reduce the value of T required to drive the exfoliation. However, this does not preclude the contribution of other physical and chemical processes; e.g., the simultaneous insertion of H into the highly stressed Si–Si bonds at the boundaries of the microcracks would also facilitate macroscopic crack propagation and lead to a consequent reduction in the measured activation energy. Clearly, a more complete treatment is
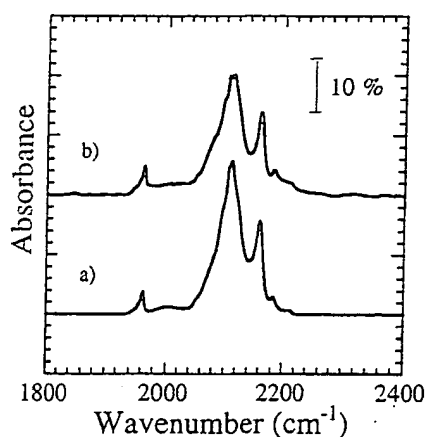
FIG. 7. Comparison of IR spectra of Si(100) implanted with 6×10^{16} H/cm^2 to a depth of 3300 Å after annealing to 475 °C for 20 min: (a) nonbonded and (b) bonded sample.

FIG. 9. Schematic illustration of (a) the blistering step and (b) the mechanical action of the handle wafer that leads to the lateral propagation of cracks.

required before a quantitative understanding can be claimed.

In the final section of this article, we will discuss the transition from blistering to complete layer transfer that occurs upon joining an implanted sample to another, handle wafer. Given the drastic nature of the change that occurs, i.e., shearing of complete 100–200 mm layers instead of formation of ~2–250 μm blisters, one might expect a significant enhancement in the development of cracks in the bonded wafer pair. In order to investigate this aspect of the process, we have annealed both bonded and nonbonded samples under identical conditions and studied the internal surface formation using both IR and TEM. Surprisingly, we find that there is essentially no difference observed between the two samples using either technique, even immediately prior to the onset of exfoliation (Figs. 7 and 8). This suggests that the effect of the bonded wafer is dynamic, in that it is only observed as the blistering/layer transfer process is occurring. Given this, we conclude that the role of the handle wafer is to provide a mechanical restoring force that opposes the vertical lift off that leads to blistering and drives lateral crack propagation instead, as schematically illustrated in Fig. 9.
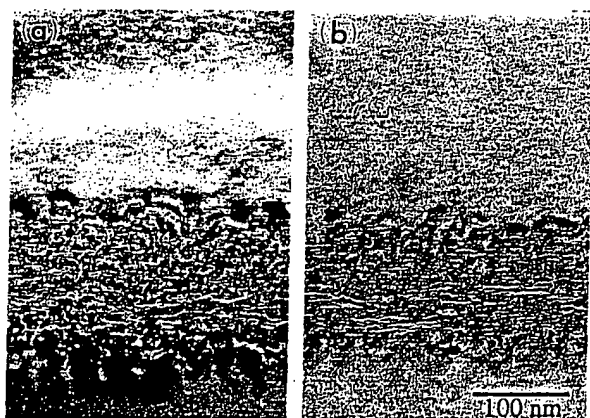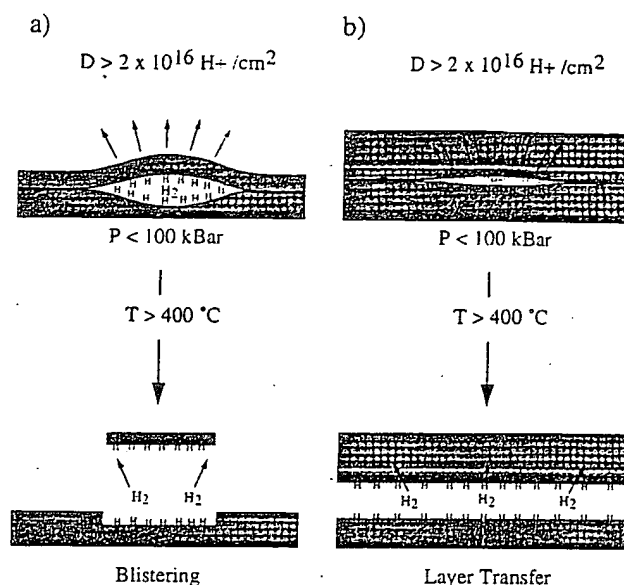
Verification of the mechanical role of the support is provided by the observation that samples implanted with hydrogen at a depth of 16 μm, show similar large-scale layer exfoliation even in the absence of the bonded "stiffener."

In summary, we have presented an overview of the extensive studies we have undertaken of the physical and chemical processes intrinsic to the hydrogen-induced exfoliation of silicon. By using a combination of techniques and a wide range of different experimental conditions, a detailed (qualitative) mechanism has begun to emerge, although much remains to be done to definitively characterize all the essential elements of this highly complex process. In particular, the predominance of the (100) internal surfaces relative to (111) and the mechanism and kinetics of the hydrogen diffusion through the implanted region need to be substantiated in order to understand the extended crack propagation and the observation that only 30% of the hydrogen contributes to the internal pressure. To this end, we are currently investigating the effect of implantation depth and annealing protocol, as well as the coimplantation of hydrogen and helium, on the evolution of the implanted region. However, many additional experimental and theoretical studies of the internal chemistry, physics, and mechanics of this process are required before a complete quantitative mechanism emerges.

FIG. 8. Comparison of TEM images of Si(100) implanted with 6×10^{16} H/cm^2 to a depth of 3300 Å after annealing to 475 °C for 20 min: (a) nonbonded and (b) bonded sample.

[1]S. J. Pearton, J. W. Corbett, and M. Stavola, Hydrogen in Crystalline Semiconductors (Springer, Berlin, 1992), and references therein.

[2]*Hydrogen in Semiconductors*, edited by J. I. Pankove and N. M. Johnson (Academic, New York, 1990).

[3]*Defects in Semiconductors 17, Materials Science Forum*, edited by H. Heinrich and W. Jantsch (Trans Tech, Switzerland, 1993), pp. 143–147.

[4]A. J. Auberton-Hervé, J. M. Lamure, T. Barge, M. Bruel, B. Aspar, and J. L. Pelloie, Silicon-On-Insulator Technology, Semi-Con West, 1995.

[5]*Proceedings of the 1st, 2nd, and 3rd International Symposia on Semiconductor Wafer Bonding: Science, Technology and Applications* (The Electrochemical Society, Pennington, NJ, 1992–1995).

[6]B. Bech Nielsen, L. Hoffmann, and M. Budde, Mater. Sci. Eng. B 36, 259 (1996).

[7]The modes above 2050 cm^{-1} had been previously assigned to either VH_y or Si_jH_y species (Ref. 1). However, following the recent definitive work of Bech Nielsen *et al.* (Ref. 8), all of these features can be attributed to VH_y species, exclusively. Therefore, the fate of the interstitials that are necessarily produced by vacancy creation is, as yet, unresolved.

[8]V. E. Marsico, M. K. Weldon, Y. J. Chabal, Y. Caudano, A. Agarwal, and D. J. Eaglesham (unpublished).

[9]Y. J. Chabal, M. A. Hines, and D. Feijoo, J. Vac. Sci. Technol. A 13, 1719 (1995); D. Feijoo, Y. J. Chabal, and S. B. Christman, Appl. Phys. Lett. 65, 2548 (1994).

[10]M. K. Weldon, Y. J. Chabal, D. R. Hamann, S. B. Christman, E. E. Chaban, and L. C. Feldman, J. Vac. Sci. Technol. B 14, 3095 (1996); M. K. Weldon, V. E. Marsico, Y. J. Chabal, D. R. Hamann, S. B. Christman, and E. E. Chaban, Surf. Sci. 368, 163 (1996).

[11]P. Dumas, Y. J. Chabal, and P. Jacob, Surf. Sci. 269/270, 867 (1992).

[12]Y. J. Chabal, G. S. Higashi, K. Raghavachari, and V. A. Burrows, J. Vac. Sci. Technol. A 7, 2104 (1989).

[13]Y. J. Chabal and K. Raghavachari, Phys. Rev. Lett. 54, 1055 (1985).

[14]The mode at 2074 cm^{-1} is the antisymmetric stretch ν_{as} of the coupled monohydride mode of steps on Si(100); the symmetric mode ν_{ss} occurs at $\sim 2087 \text{ cm}^{-1}$ [P. Jakob and Y. J. Chabal, J. Chem. Phys. 95, 2897 (1991)] and cannot therefore be resolved from the tail of the 2091 cm^{-1} feature. The mode at 2098 cm^{-1} in the 650 °C spectrum is the ν_{ss} of the coupled monohydride on the flat (100) terraces; the antisymmetric component is not observed due to the decreased relative sensitivity to such "parallel" modes upon developing micron-sized internal cracks (Ref. 10).

[15]G. S. Higashi, Y. J. Chabal, G. W. Trucks, and K. Raghavachari, Appl. Phys. Lett. 56, 656 (1990).

[16]N. M. Johnson, F. A. Ponce, R. A. Street, and R. J. Nemanich, Phys. Rev. B 35, 4166 (1987); H. P. Strunk, H. Cerva, and E. G. Mohr, J. Electrochem. Soc. 135, 2876 (1989).

[17]P. Deák, L. C. Snyder, and J. W. Corbett, Phys. Rev. B 37, 6887 (1988).

[18]A. J. Leadbetter, A. A. M. Rashid, N. Colenutt, A. F. Wright, and J. C. Wrights, Solid State Commun. 38, 957 (1981).

[19]H. J. Stein, S. M. Myers, and D. M. Follstaedt, J. Appl. Phys. 73, 2755 (1993).

[20]Q.-Y. Tong, T.-H. Lee, K. Gutjahr, S. Hopfe, and U. Gösele (unpublished).